Numerical Simulation of Crack Evolution Under Hydraulic Fracturing of Medium-Hard Rock

Jialiang Liu, Jinyang Li, Yujie Zhu, Dongping Zhou, Hua He, Junjie Zhou, and Kai Wang

Abstract The mechanical excavation technology, as a commonly used method in tunnel excavation of hard rock, has many shortcomings, such as poor geological adaptability and intense wear of cutter head and so on, affecting the excavation efficiency. The hydraulic fracturing technology can effectively evade these issues and achieve the efficient excavation by pre-fracturing rock. Therefore, taking medium-hard rock as an example, this paper established the numerical models of single-borehole and double-borehole hydraulic fracturing medium-hard rock based on the extended finite element method (XFEM), and explored the evolution law of cracks and the damage dissipation energy variation of the rock. Results indicated that under single-borehole hydraulic fracturing, the propagation length and width of the crack experienced the rapid growth period and slow growth period, and the damage dissipation energy of rock mainly experienced the step-like growth period. By the comparative analyses of crack propagation length and width evolution as well as the damage dissipation energy of rock under the single-borehole and double-borehole hydraulic fracturing, it is found that under the double-borehole hydraulic fracturing the propagation rate and damage dissipation energy of single prefabricated fracture are greatly in-creased, and the fracturing efficiency is greatly improved, compared with the single-borehole hydraulic fracturing. Results can provide a theoretical reference for improving the application level of hydraulic fracturing in tunnel excavation.

D. Zhou (✉) · J. Zhou · K. Wang
Chongqing Energy Investment Group Science & Technology Co., LTD.,
Chongqing 400061, People's Republic of China
e-mail: dpzcq2001@163.com

J. Liu · J. Li · Y. Zhu
Civil Engineering College, Chongqing Jiaotong University,
Chongqing 400074, People's Republic of China

H. He
Chongqing Energy Investment Group Co., LTD.,
Chongqing 401121, People's Republic of China

S. N. Atluri and I. Vušanović (eds.), *Computational and Experimental Simulations in Engineering*, Mechanisms and Machine Science 98,
https://doi.org/10.1007/978-3-030-67090-0_18

Keywords Hydraulic fracturing · Medium-hard rock · Crack; Borehole · Numerical simulation

1 Introduction

The exploitation and excavation of the various underground resources usually encounter many problems, especially the hard rock layer problems such as high density, poor breaking conditions and so on. Usually, the mechanical drilling tool is used in the tunneling excavation, but the geological adaptability is poor and the wear of the hard rock to the drilling tool causes the frequent replacement of cutting head, thereby engendering the high cost and low efficiency. Therefore, it is urgent to take efficient measures to achieve the efficient excavation of hard rock [1]. Hydraulic fracturing technology was widely applied in the field of geotechnical engineering [2–4]. The technology can reduce the hardness and integrity of the rock by crack initiation and expansion, which greatly reduces the loss of the tool head and promotes the mechanical tunneling of rock.

Recently, many scholars have carried out a large number of experiments and numerical simulation studies on the hydraulic fracturing. Nasehi [5] et al. performed the numerical simulation of hydraulic fracturing rock and analyzed the effects of in-situ stress and strength parameters of intact rock on the fracturing properties based on the discrete element method. By the extended finite element method (XFEM), Tian [6] et al. simulated the processes of continuous fracturing, the alternative fracturing and the improved zipper hydraulic fracturing, and studied the effects of the in-situ stress difference and the crack spacing on crack propagation. Shimizu et al. [7] discussed the influence of fluid viscosity and rock granularity on hydraulic fracturing by means of discrete element method. Francisco et al. [8] made a significant prediction concerning the coupling crushing behavior of the hydraulic fracturing rock based on the extended finite element method, and analyzed the interaction between the hydraulic crack and the natural crack. By the Cohesive units, Xue et al. [9] studied the relationship between the fluid pressure on the crack surface and the crack propagation as well as fluid percolation. The effect of fluid pressure on the width variation of crack during the crack propagation was studied by Ji et al. [10]. Shilova [11] et al. explored the influence of wellbore and crack radius on initiation pressure of crack and crack propagation by the hydraulic fracturing experiment of rock.

The above-mentioned scholars had made great progress in the effects of the in-situ stress difference, rock strength and natural cracks on the crack propagation of rock under hydraulic fracturing, but there are few influence researches of the borehole and its arrangement on the crack propagation. The borehole has a significant effect on the energy dissipation in rock and crack propagation under hydraulic fracturing, which influences the rock crushing efficiency. Hence, the numerical models of hydraulic fracturing medium-hard rock with single and double boreholes were established based on the XFEM. And it systematically explored the

evolution law of crack propagation length, width and rate as well as damage dissipation energy under the working conditions of single-borehole and double-borehole. The study is expected to more deeply reveal the crack propagation law under porous fracturing of medium-hard rock and provide a potent reference for the actual hydraulic fracturing construction in tunnel excavation.

2 Numerical Simulation

2.1 Basic Hypotheses and Theories

In the process of hydraulic fracturing, the basic assumptions for the establishment of the two-dimensional numerical model are as follows [12]: 1) the model is isotropic and homogeneous limestone; 2) only the hydraulic effect in the two-dimensional plane is considered, ignoring the vertical flow of the fluid; 3) the fluid in the model is single-phase and incompressible; 4) the model of rock is incompressible; 5) the influence of gravity is not considered.

For the two-dimensional model, the Griffith strength theory under biaxial stress can be expressed as:

$$P_{\mathrm{t}}=\frac{(\sigma_1-\sigma_3)^2}{8(\sigma_1+\sigma_3)},\ \frac{\sigma_3}{\sigma_1}\geq-\frac{1}{3} \tag{1}$$

$$P_t=-\sigma_3\ \frac{\sigma_3}{\sigma_1}\leq-\frac{1}{3} \tag{2}$$

In the formula, σ_1 and σ_3 are the maximum and minimum principle stress respectively, P_t is the compressive strength.

2.2 Model Establishment

Taking limestone as the simulation model of medium-hard rock, the two-dimensional models were established to simulate the actual conditions (Fig. 1). The mechanical parameters of the models are shown in Table 1. In the models, prefabricated fractures were simulate by inserting spread function, and the boreholes of fracturing fluid on the prefabricated fractures were selected. The maximum circumferential stress criterion of crack initiation and damage evolution criterion were introduced to determine the crack initiation and damage evolution of element [13]. Therefore, two analysis steps were established in the process of single-borehole hydraulic fracturing: the one was the in-situ stress balance stage, the other was the hydraulic fracturing stage. For the double-borehole hydraulic fracturing, it was distributed to four analysis steps: the first one was the in-situ stress

balance stage, the second one was the hydraulic fracturing stage of borehole I, the third one was the unload stage of borehole I, and the fourth one was the hydraulic fracturing stage of borehole II.

The minimum and maximum principal in-situ stress of the rock model were 6 MPa and 15 MPa respectively, and the initial void ratio was 0.1. The viscosity of water as fracturing liquid was 0.001 Pa•s. The unit weight of water was 9800 N/m^3. The constraint boundary conditions were set to fix the dis-placement in X and Y directions. The initial pore pressure was 0, with the perforation angle of 60°. The initial time step at the hydraulic injection stage was 0.1 s, with the injection time of 100 s. And, the water pressure of hydraulic fracturing was 30 MPa.

2.3 Control Equation

The crack growth under hydraulic fracturing is caused by the expansion of fluid pressure and shear displacement effect, so the crack under hydraulic fracturing is composite crack. The failure cohesion model was established by XFEM method to study the crack initiation and propagation criterion of the composite crack, and the main analyzed contents contained the functional response relationship between the interface tensile stress and the relative displacement of the interface, as well as the relationship between the interface energy in the failure process.

In the process of hydraulic fracturing, as the injection of the fracturing fluid, the seepage pressure of the fluid acting on the crack surface increased, which led to the increase of fluid loss to the rock and the change of the stress state in the crack. Whereas the stress change will inevitably cause the change of the parameters such as the porosity of the medium-hard rock and the seepage velocity of the fluid. Conversely, the stress change has the important influence on the seepage pressure

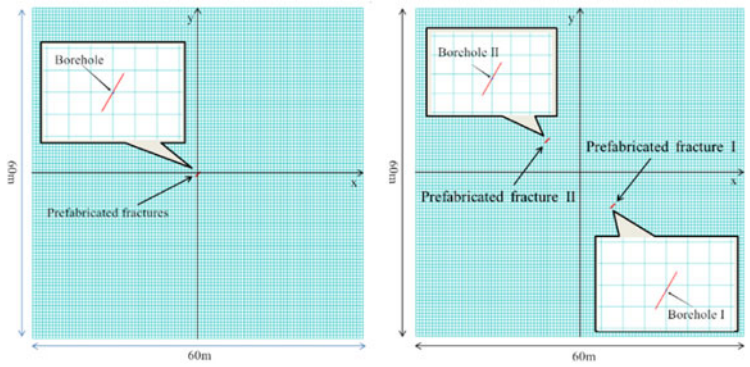

Fig. 1 Two-dimensional geometric model of hydraulic fracturing limestone

Table 1 Mechanical parameters of limestone model

Elastic Modulus / GPa	Poisson's ratio	Porosity ratio	Permeability coefficient	Filtration coefficient	Tensile strength/MPa
15	0.25	0.1	1×10^{-7}	1×10^{-14}	6

of the fluid. The interaction between the fluid seepage and the rock deformation in medium-hard rock is called the seepage-stress coupling [14].

The equilibrium equation of solid rock [9]:

$$\int_V (\overline{\sigma} - P\mathrm{w}I) : \delta_\varepsilon dV = \int_S \hat{T}\delta u dS + \int_V \hat{f}\delta u dV \tag{3}$$

The continuity equation of seepage liquid:

$$\frac{d}{dt}\left(\int_V n dV\right) = -\int_S n\overrightarrow{\mathrm{n}} v_w dS \tag{4}$$

Critical stress criterion of element damage:

$$\max\left\{\frac{\langle\sigma_\mathrm{n}\rangle}{\sigma_\mathrm{n}^0}, \frac{\sigma_\mathrm{s}}{\sigma_\mathrm{s}^0}, \frac{\sigma_\mathrm{t}}{\sigma_\mathrm{t}^0}\right\} = 1 \tag{5}$$

Linear degradation criterion of elastic modulus is represented as follows.

$$E = (1 - D)E_0 \tag{6}$$

$$D = \frac{\delta_m^f(\delta_m^{\max} - \delta_m^0)}{\delta_m^{\max}(\delta_m^f - \delta_m^0)} \tag{7}$$

In these formulas, δ_ε, $\overline{\sigma}$, $\hat{T}$, $\hat{f}$ and δu are the virtual strain, effective stress, surface force, unit volume force and displacement except gravity, respectively. v_w, $\overrightarrow{\mathrm{n}}$ and n are the seepage velocity of the fluid in the solid, the unit vector in the normal direction of the surface S and the porosity, respectively. σ_n is the normal stress, σ_s and σ_t are the tangential stress (in two dimensions, $\sigma_\mathrm{t} = 0$), σ_n^0 is the threshold stress of normal damage, σ_s^0 and σ_t^0 are the threshold stresses of tangential damage.E_0, E, D, $\delta_m^{\max}$ and δ_m^0 are the Young's modulus of the undamaged and damaged element, the damage factor, the maximum displacement of the element in the loading process, and the opening displacement when it reaches the damage.

3 Results and Discussion

3.1 Propagation Analysis of Prefabricated Fracture Under Single-Borehole Hydraulic Fracturing

With the continuous injection of high pressure fluid into limestone, the internal pressure of the limestone increased gradually, and the concentrated cluster formed in the perforation, which caused the crack initiation along the direction of the prefabricated fractures. When the pressure increased to a certain value, the prefabricated fracture evolved into the wide fracture. As the high-pressure fluid entered into the fracture, the fluid reached the fracture tip and the fracture continued to expand. Simultaneously, the continuous expansion of the fracture caused the decrease of the stress concentration at the crack tip. The crack propagation versus time is shown in Fig. 2. There was an energy accumulation period of crack propagation, and the prefabricated fracture propagated at t = 5 s. The crack extended along both positive and negative directions of Y-axis. Due to the restriction of the maximum and minimum horizontal in-situ stresses, the crack expansion length in the positive negative directions of Y-axis was larger than that in the negative directions of Y-axis.

The change curves of crack length and the maximum width with time are shown in Fig. 3. Before t = 5 s, the crack length and width have no obvious change. The stage from t = 5 s to t = 20 s was the rapid growth period of the crack propagation length. The stage from t = 20 s to t = 100 s was the slow growth period of the crack propagation length, and the propagation length tended to be stable at the terminal stage. For the crack propagation width, the stage from t = 5 s to t = 25 s was the rapid growth period of crack propagation width, and the stage from t = 25 s to t = 100 s was the slow growth period of crack propagation width. The detailed process of crack propagation is as follows: From t = 5 s to t = 20 s, the propagation length of the crack increased from 1.58 m to 9.56 m at an average rate of 0.550 m/s, and from 20 to 100 s, the propagation length of the crack increased from 9.56 m to 22.02 m at an average rate of 0.156 m/s; from 5.5 s to 25 s the propagation width of the crack increased from 1.152 mm to 2.223 mm at an average rate of 0.055 mm/s, and from 25 to 100 s, the propagation width of the crack increased from 2.223 mm to 3.355 mm at an average rate of 0.015 mm/s.

It is obvious that both the transverse and longitudinal propagation rates of the prefabricated fracture first sharply increased and then slowly increased. This is because that as the high pressure fluid enters the prefabricated fracture, the fluid pressure in the crack begins to increase. And the propagation rate of the crack increases at a sharp speed due to the stress concentration at the crack tips, hence the expansion rate of the crack increased rapidly. Whereas, as the crack length expanded to a certain length, the fluid pressure reached the peak value of 57.22 MPa, and the pressure began to decrease, finally it dropped to 23.74 MPa at t = 100 s (Fig. 4), thereby the expansion rate of the crack increased slowly.

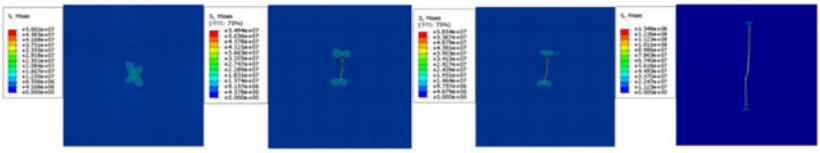

(a) t=5 s (b) t = 20 s (c) t = 25 s (d) t = 100 s

Fig. 2 The prefabricated fracture propagation nephogram under single-borehole hydraulic fracturing at different time

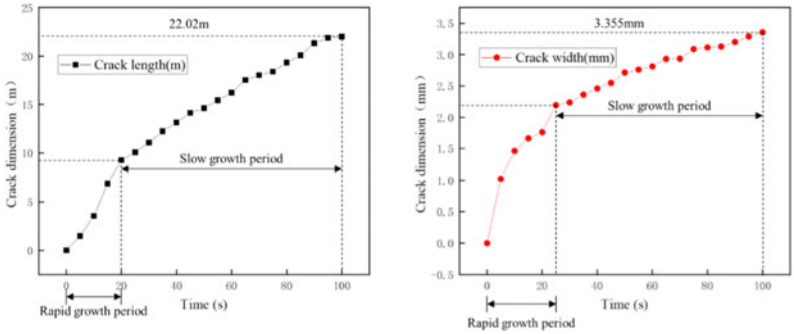

(a) Propagation length (b) Maximum width

Fig. 3 The change curve of propagation length and maximum width of prefabricated fracture under single-borehole hydraulic fracturing with time

The higher the damage dissipation energy of rock is, the larger the fragmentation degree of the rock is [15, 16]. The energy dissipation process reflects the evolution of rock damage under hydraulic fracturing. By the change curve of damage dissipation energy of rock with time in Fig. 5, the stage from t = 0 s to t = 5 s was the energy accumulation period, the damage dissipation energy of rock was 0. The stage from t = 5 s to t = 22 s was the rapid energy development period where the damage dissipation energy of rock increased rapidly and reached a certain threshold value. And the stage from t = 22 s to t = 100 s was the step-like growth period of energy where the damage dissipation energy increased as the time increased. The maximum damage dissipation energy of rock was 46.1 kJ in the whole fracturing process.

3.2 *Propagation Analysis of Prefabricated Fractures Under Double-Borehole Hydraulic Fracturing*

Under double-borehole hydraulic fracturing, the spacing of the two prefabricated fractures was set as 15 mm, which can effectively improve the fracturing effect of rock [17]. The numerical simulation of double-borehole hydraulic fracturing was divided into two stages: the first one was the hydraulic fracturing of borehole I for 100 s, the second one was the hydraulic fracturing of borehole II for 100 s. The crack propagation process is shown in Fig. 6. The prefabricated fracture I first initiated and expanded, and the prefabricated fracture II had simultaneously occurred crack initiation and propagation due to the influence of propagation stress field of prefabricated fracture I. The propagation characteristics of prefabricated fracture I under double-borehole hydraulic fracturing were basically same as that under single-borehole fracturing. For the prefabricated fracture II, it initiated and expanded at t = 5 s. From t = 5 s to t = 30 s, the propagation length of the crack increased from 1.27 m to 10.92 m at an average rate of 0.386 m/s, and the propagation width of the crack increased from 1.09 mm to 3.53 mm at an average rate of 0.098 mm/s. From 30 to 100 s, the propagation length of the crack increased from 10.92 m to 17.60 m at an average rate of 0.095 m/s, and the propagation width of the crack increased from 3.53 mm to 5.45 mm at an average rate of 0.027 mm/s.

By the statistical analysis of the simulation results, the change laws of the propagation length and maximum width of the prefabricated fracture II under double-borehole hydraulic fracturing with time were obtained. According to Fig. 7, the maximum propagation length of the prefabricated fracture II was 17.6 m at t = 100 s, which decreased by 25.1% than that of single-borehole hydraulic fracturing. The maximum propagation width of the prefabricated fracture II was 5.453 mm, which increased by 62.5% than that of hydraulic fracturing with single-borehole hydraulic fracturing. Due to the stress interference of the

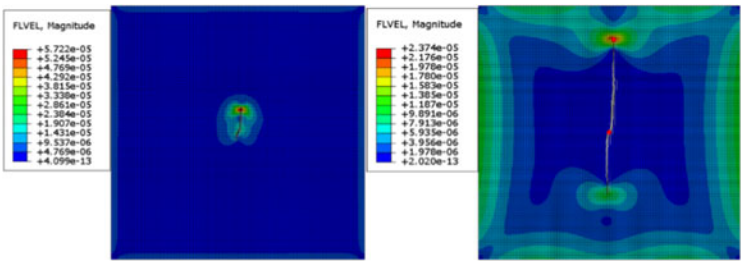

(a) Nephogram of maximum fluid pressure (b) Nephogram of fluid pressure at t = 100s

Fig. 4 Fluid pressure distribution at the prefabricated fracture tip under single-borehole hydraulic fracturing

prefabricated fracture I to prefabricated fracture II, the propagation rate of prefabricated fracture II under double-borehole hydraulic fracturing is increased by 10.49%, compared with that under single-borehole hydraulic fracturing.

According to the variation law of damage dissipation energy of rock with time in Fig. 8, the stage before $t = 7$ s was the energy accumulation period of prefabricated fractures I and II. The stage from $t = 7$ s to $t = 90$ s was the step-like growth period of energy. And the stage from 90 to 100 s was the steady development period where the energy was almost constant with the increase of time. The maximum damage dissipation energy is 163.1 kJ in the whole process, which is at least 3.5 times of that under double-borehole hydraulic fracturing, thereby the fragmentation

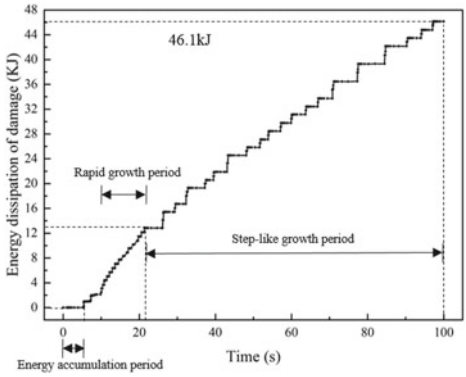

Fig. 5 Change curve of damage dissipation energy of limestone under single-borehole hydraulic fracturing with time

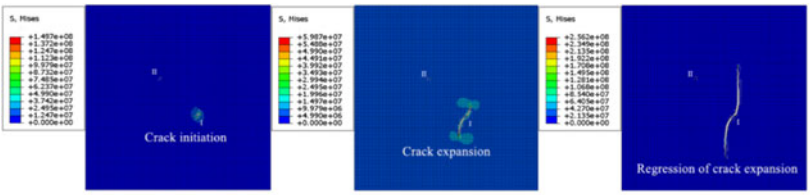

(a) $t = 5$ s (b) $t = 30$ s (c) $t = 100$ s

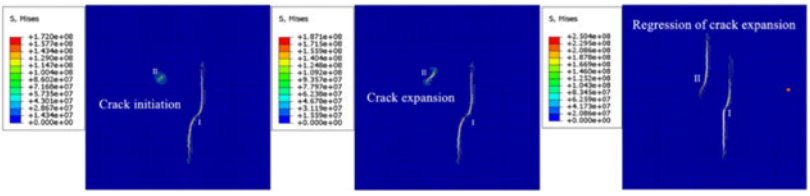

(d) $t = 5$ s (e) $t = 30$ s (f) $t = 100$ s

Fig. 6 The prefabricated fracture propagation nephogram under double-borehole hydraulic fracturing at different time. (The Fig. 6(a), Fig. 6(b) and Fig. 6(c) are the nephogram at the first stage, the Fig. 6(d), Fig. 6(e) and Fig. 6(f) are the nephogram at the second stage)

degree of rock under double-borehole hydraulic fracturing is larger than that under single-hole hydraulic fracturing. This is because the hydraulic fracturing of borehole I has the promoting effect to the fracturing of borehole II. In the process of double-borehole hydraulic fracturing, due to the stress interference between the two cracks, there will be a stress interaction zone between the two cracks, which benefits the prefabricated fractures to propagate in different directions and different degrees. Therefore, under the double-borehole hydraulic fracturing, the damage dissipation energy of prefabricated fracture II are greatly increased, and the fracturing efficiency is greatly improved under double-borehole hydraulic fracturing, compared with the single-borehole hydraulic fracturing.

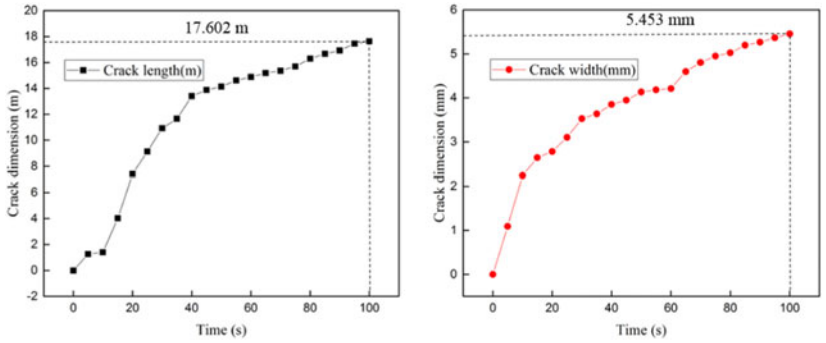

(a) Propagation length (b) Maximum width

Fig. 7 The change curve of propagation length and maximum width of prefabricated fracture II under double-borehole hydraulic fracturing with time

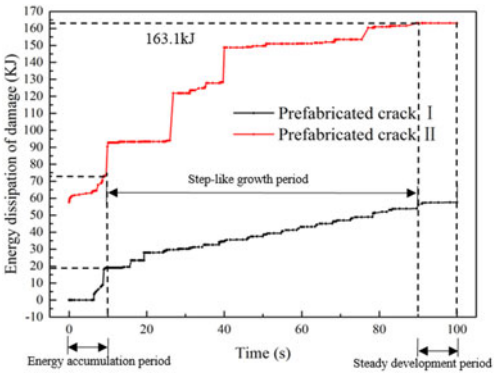

Fig. 8 Change curve of damage dissipation energy of rock with double-borehole prefabricated fracture with time

4 Conclusion

On the basis of XFEM, this paper established the numerical models of single-borehole and double-borehole hydraulic fracturing medium-hard rock, and comparatively analyzed the evolution law of crack and the damage dissipation energy of rock under the single-borehole and double-borehole hydraulic fracturing. The main conclusion is concluded as follows:

(1) Under the single-borehole and double-borehole hydraulic fracturing, the propagation lengths and widths of the prefabricated fracture as well as the damage dissipation energy of rock increase with the increase of time. And the crack propagation length and width experience both the rapid growth period and the slow growth period, and the damage dissipation energy of rock mainly appears the step-like increase continuously.
(2) Because of the promotion effect of early borehole hydraulic fracturing to later borehole hydraulic fracturing, under the double-borehole hydraulic fracturing, the propagation length of single prefabricated fracture is reduced by 25.1%, and the propagation width is increased by 62.5%, compared with single-borehole hydraulic fracturing. By the comparative analysis of damage dissipation energy of rock under hydraulic fracturing of the single and double boreholes, the damage dissipation energy of single prefabricated fracture under the double-borehole hydraulic fracturing is increased by at least 3.5 times than that of single-borehole hydraulic fracturing. It can be concluded that the fracturing efficiency of single prefabricated fracture under the double-borehole hydraulic fracturing is higher than that under single-hole hydraulic fracturing.

References

1. Muther, T., Khan, M.J., Chachar, M.H., et al.: A Study on designing appropriate hydraulic fracturing treatment with proper material selection and optimized fracture half-length in tight multilayered formation sequence. SN Appl. Sci. **2**(5), 1–12 (2020)
2. Legarth, B., Huenges, E., Zimmermann, G., et al.: Hydraulic fracturing in a sedimentary geothermal reservoir: Results and implications. Int. J. Rock Mech. Min. Sci. **42**, 1028–1041 (2005)
3. Fomin, S., Hashida, T., Shimizu, A., et al.: Fractal concept in numerical simulation of hydraulic fracturing of the hot dry rock geothermal reservoir. Hydrol. ProcHydrological Processesrnesses **17**(14), 1–15 (2003)
4. Damjanac, B., Cundall, P.: Application of distinct element methods to simulation of hydraulic fracturing in naturally fractured reservoirs. Comput. Geotech. **71**, 283–294 (2016)
5. Nasehi, M.J., Mortazavi, A.: Effects of in-situ stress regime and intact rock strength parameters on the hydraulic fracturing. J. Petrol. Sci. Eng. **108**, 211–221 (2013)
6. Wei, T., Peichao, L., Yan, et al.: Numerical simulation of sequential, alternate and modified zipper hydraulic fracturing in horizontal wells using XFEM. J. Petrol. Sci. Eng. (183), 106251 (2019)

7. Shimizu, H., Murata, S., Ishida, T.: The distinct element analysis for hydraulic fracturing in hard rock considering fluid viscosity and particle size distribution. Int. J. Rock Mech. Min. Sci. **48**(5), 712–727 (2011)
8. Francisco, C., Deane, R., do Amaral Vargas Jr., E.: An XFEM implementation in Abaqus to model intersections between fractures in porous rocks. Comput. Geotech. (112), 135–146 (2019)
9. Xue, B., Zhang, G., Wu, H., et al.: Three-dimensional numerical simulation of hydraulic fracture in oil wells. J. Univ. Sci. Technol. China **38**(11), 1322–1325 (2008). 1347. (in Chinese)
10. Ji, S.-H., Koh, Y.-K., Kuhlman, K.L., et al.: Influence of pressure change during hydraulic tests on fracture aperture. Ground Water (51), 298–304 (2013)
11. Tatjana, S., Andrey, P., Leonid, R., et al.: Development of the impermeable membranes using directional hydraulic fracturing. In: Symposium of the International Society for Rock Mechanics, no. 191, pp. 520–524 (2017)
12. Xing, J., Hou, Li., Zhang, T.: Numerical simulation of the whole process of hydraulic fracturing under different directional fractures. Water Conservancy Technical Supervision (6), 175–179 (2019). (in Chinese)
13. Liang, B., Yue, L., Sun, W.: The influence of shale mineral composition on crack growth: numerical simulation. Marine Petrol. Geol. 24(4), 97–101(2019). (in Chinese)
14. Zhang, R., Wang, Q., Zhang, Z., et al.: Research of ABAQUS numerical simulation of 3D fracture propagation in hydraulic fracturing process. Oil Drill. Prod. Technol. **34**(6), 69–72 (2012). (in Chinese)
15. Wang, L., Gao, Q.: Fragmentation distribution prediction of rock based on damage energy dissipation. Chin. J. Rock Mech. Eng. **26**(6), 1202–1211 (2007). (in Chinese)
16. Xia, C., Ju, Y., Xie, H.: Numerical analysis of propagation of explosion wave and energy dissipation in tunnel and surrounding rockmass. J. Ballistics **17**(4), 1–5 (2005). (in Chinese)
17. Li, S., Ren, Y., Fan, C., et al.: Influence of spacing between boreholes on hydraulic fracturing to enhance coal seam gas extraction. J. Safety Sci. Technol. **14**(1), 70–76 (2018). (in Chinese)